Preprint
UCRL-JC-145248

Practical High-Order Adaptive Optics Systems for Extrasolar Planet Searches

B. Macintosh, S. Olivier, B. Bauman, J. Brase, E. Carr, C. Carrano, D. Gavel, C. Max, J. Patience

This article was submitted to SPIE's 46th Annual Meeting International Symposium on Optical Science and Technology, San Diego, CA, July 29 – August 3, 2001 .

U.S. Department of Energy

Lawrence Livermore National Laboratory

August 29, 2001

Practical high-order adaptive optics systems for extrasolar planet searches

Bruce A. Macintosh*, Scot Olivier, Brian Bauman, James Brase, Emily Carr, Carmen J. Carrano, Donald Gavel, Claire E. Max, Jennifer Patience
Lawrence Livermore National Laboratory

ABSTRACT

Direct detection of photons emitted or reflected by an extrasolar planet is an extremely difficult but extremely exciting application of adaptive optics. Typical contrast levels for an extrasolar planet would be 10^9 – Jupiter is a billion times fainter than the sun. Current adaptive optics systems can only achieve contrast levels of 10^6, but so-called "extreme" adaptive optics systems with 10^4 -10^5 degrees of freedom could potentially detect extrasolar planets. We explore the scaling laws defining the performance of these systems, first set out by Angel (1994), and derive a different definition of an optimal system. Our sensitivity predictions are somewhat more pessimistic than the original paper, due largely to slow decorrelation timescales for some noise sources, though choosing to site an ExAO system at a location with exceptional r_0 (e.g. Mauna Kea) can offset this. We also explore the effects of segment aberrations in a Keck-like telescope on ExAO; although the effects are significant, they can be mitigated through Lyot coronagraphy.

Keywords: adaptive optics, astronomy, extrasolar planets

1. "EXTREME" ADAPTIVE OPTICS

Direct detection of photons from extrasolar planets is one of the most exciting applications of large telescopes. By contrast to highly-successful indirect detection technique[1], which measures orbital parameters and indirectly constrains mass, a *direct* detection of Jupiter-sized planets could lead to photometric or spectroscopic measurements of an object's radius, temperature, and composition, and is a crucial step on the road towards detection of Earthlike planets, particularly since it is most sensitive to solar systems that resemble our own.

Direct detection is of course extremely challenging. Current adaptive optics (AO) systems can achieve contrast levels of ~10^6 at moderate (~1") separations[2], sufficient to detect young (<20 MYr) extrasolar planets in wide orbits through near-infrared thermal emission. A mature planet such as Jupiter, though, is approximately 10^9 fainter than its parent star – far beyond the reach of current AO or space telescopes. Angel (1994)[3] , in an important paper setting out

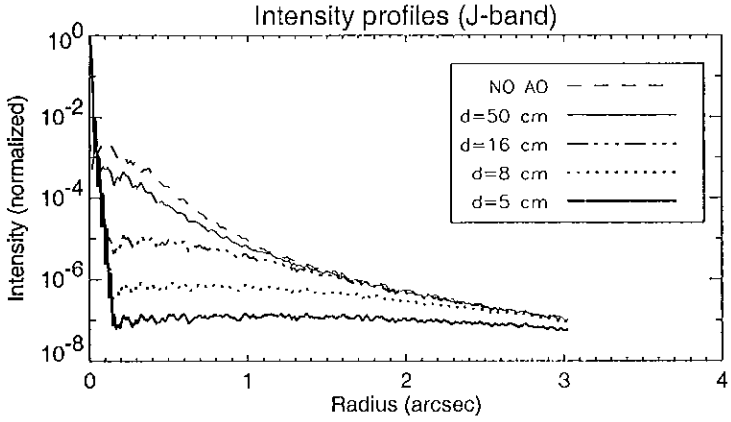

Figure 1: Simulated ExAO profiles in the ideal case with no wavefront sensing noise

* bmac@igpp.ucllnl.org; phone 925-423-8129; Lawrence Livermore National Laboratory, L-413, 7000 East Ave., Livermore, CA 94551

the fundamental scaling laws and limitations, recognized that a ultra-high-contrast AO system with 10^4 degrees of freedom could begin to achieve these contrast levels. A follow-on paper[4] presented simulations of these systems.

With high-speed computers, better wavefront sensors, and the development of micro-electro-mechanical (MEMS) deformable mirrors, the technologies needed to construct such systems are now beginning to become available. The NSF Center for Adaptive Optics (CfAO) has begun a study of possible ultra-high-contrast AO systems, an area dubbed "extreme" adaptive optics[5], or ExAO. These can be defined as AO systems whose primary concern is not improving the central peak – their Strehl ratio will already be very close to one – but surpressing the halo of scatted light that surrounds any AO-corrected star; the figure of merit is no longer Strehl ratio but $(1\text{-Strehl})^{-1}$ – the intensity of the residual halo – or the normalized gain G defined by Angel (see section 2.) ExAO systems have a characteristic PSF with a sharp peak and a relatively flat halo out to a "control radius" given by λ/d, where d is the actuator spacing or subaperture size. Figure 1 shows a family of performance curves for such systems in an ideal case where only finite actuator spacing limits performance.

Target planets will almost always be fainter than even the most extreme of ExAO halos, so the ability to detect the small deviation in the halo caused by a planet depends on the smoothness of the halo. In instantaneous images the halo is completely non-smooth, consisting of a pattern of diffraction-limited speckles, but over long exposures these speckles move around and average out.

The current goal of the CfAO ExAO project is a conceptual design for such a system for deployment on a 5-10 m telescope. Crucial questions include:

1. Noise scaling: what is the optimal subaperture size d and update rate Δt?
2. Speckle decorrelation: how fast do the residual speckles that compose the halo decorrelate and smooth out?
3. Scintillation control: to what level do intensity fluctuations in the pupil need to be controlled, and what is the best technology to do this with?
4. Practical manufacture: what technologies can be used to build these systems?
5. Telescope choice: what effects to issues such as telescope segmentation and site quality (r_0) have?

This paper will present preliminary studies that address issues 1,2, 4 and 5. Scintillation was studied in the original papers by the Arizona group[3,4] and will not be addressed here. Overall, we derive somewhat different system optimizations than Angel, and performance predictions that are somewhat more pessimistic, due largely to the slow decorrelation timescale of some residual image speckles. In spite of these pessmistic assumptions, it still seems possible that ExAO systems could reach planet-detection contrast levels, particularly on a 8-10m telescope at a site with good r_0.

2. SYSTEM OPTIMIZATION AND NOISE SCALING

2.1 System optimization in Angel 1994

In his original paper, Angel[3] defines a normalized system gain, G, which is the ratio of the peak intensity to the halo intensity; since these systems generally operate at strehl ratio of 1, the gain G is given by

$$G = \frac{1}{\sigma^2} \cdot \frac{D^2}{d^2} \tag{1}$$

where D is the telescope diameter and σ^2 is the total wavefront variance. In the ideal case, σ^2 can be broken down into three irreducible terms, which we will designate σ^2_{wfs}, σ^2_{fit}, σ^2_{bw}, corresponding to noise (primarily due to photon statistics) in the measurement of the wavefront, errors due to imperfect sensing and correcting of the wavefront caused by finite subaperture size, and a bandwidth error term due to the finite timestep over which the atmospheric wavefront is sensed. It is important to note that this treats only the errors in the sensing process, in an idealized case in which a perfect wavefront corrector responds instantaneously, and only the finite signal to noise, spacing, and temporal resolution of the sensor contributes. This allows Angel to develop the "best-case" scenario, since while correctors and computers may achieve very high performance levels in the future, the sensing error sources can never be reduced. Angel derives expressions for each of these terms as follows

$$\begin{aligned} \sigma^2 &= \sigma^2_{wfs} + \sigma^2_{fit} + \sigma^2_{bw} \\ &= \frac{1}{F_s q \Delta t d^2} + \left(g\frac{d}{r_0}\right)^{5/3} + \left(w\frac{\Delta t}{r_0}\right)^{5/3} \end{aligned} \tag{2}$$

where F_s is the flux from the target star, q is a generalized quantum efficiency and illumination term for the WFS, g is a geometric term for the sensing/correcting geometry, and w is a generalized turbulence-weighted wind velocity multiplied

by a scaling factor. Typical values would be F_s=10^9 photons/m^2/second, q=0.2 for the interferometric wavefront sensor described by Angel, g=0.4 for square subapertures, and w=32 m/s for wind velocity v=10 m/s.

Angel then derives an "optimal" system design (d and Δt) for a given star brightness, by minimizing the total σ^2. For a target star with R-band magnitude m_R varying from 3.8 to 0.0, the optimal d varies from 4.3 to 2.2 cm. With this optimum (which in Angel's formalism is independent of telescope diameter) he calculates signal to noise ratios for various telescope and star combinations. Angel assumes that the halo is completely speckled but that these speckles randomize themselves between each AO timestep Δt, and hence the signal-to-noise is given by

$$SNR = \frac{G\sqrt{T_{int}/\Delta t}}{F_S/F_P} \tag{3}$$

where T_{int} is the total integration time and F_p is the flux from the target planet. (As will be seen in section 3, this assumption of rapid speckle decorrelation may not be true.)

2.2 System optimization in this paper

Equation 3 shows that (assuming perfect speckle decorrelation) the key parameter in planet detection is not σ^2 but G – not the total wavefront error, but the halo intensity. Hence an optimal system could be considered to be one that maximizes G. Maximizing G is equivalent to minimizing $\sigma^2 d^2$. For a fixed σ, decreasing d reduces the average halo intensity by decreasing the minimum spatial frequency that can be controlled in the final image – in effect, spreading a finite amount of light over a larger control radius. We therefore wish to minimize equation 4, below; which monotonically decreases with decreasing d. In effect, the "optimum" system in this ideal case occurs at d=0. This occurs because the only wavefront error term that increases with smaller d is the measurement photon noise term, which scales as d^{-2}. As d decreases the measurement noise increases but the resulting halo intensity is spread over a larger area.

$$\begin{aligned}\sigma^2 d^2 &= \left(\sigma^2_{wfs} + \sigma^2_{fit} + \sigma^2_{bw}\right)d^2 \\ &= \left(\frac{1}{F_s q \Delta t d^2} + \left(g\frac{d}{r_0}\right)^{5/3} + \left(w\frac{\Delta t}{r_0}\right)^{5/3}\right)d^2 \\ &= \frac{1}{F_s q \Delta t} + \left(g\frac{d^{11/3}}{r_0^{5/3}}\right) + \left(w\frac{\Delta t}{r_0}\right)^{5/3} d^2\end{aligned} \tag{4}$$

The non-physical optimum at d=0 applies only in the case of a wavefront sensor with only photon noise. Finite readout noise in the wavefront sensor adds a d^4 dependence to σ^2_{wfs} and shifts the optimization to small but finite d, ~1 cm for m_R=0. When the effects of persistent speckles are included (Section 3) it becomes appropriate to optimize on the final signal to noise ratio rather even than G, which leads to optimum d<1cm even for m_R=4.0. In a practical system, d will be limited by wavefront corrector technology and the "best" ExAO system will usually be the one with the highest possible actuator count.

3. SPECKLE DECORRELATION TIMESCALES

3.1 Speckle decorrelation simulations

The residual halo, if seen in an instantaneous monochromatic image, is completely composed of individual speckles (see Figure 2a for a representative example). These speckles are significantly brighter than any mature extrasolar planet is likely to be. To detect a planet, we must integrate long enough that multiple realizations of the speckles average out and result in a smooth image. Speckles in uncorrected (but tilt-removed) astronomical images or outside the AO control radius persist over a timescale t_{spec} = 50-200 ms ≈ 0.3 D/v.[6]. This time can be thought of as the clearing time for a substantial fraction of a phase screen to move over the telescope pupil. Other analyses of speckle decorrelation, such as the multilayer analysis by Roddier[7], suggest that this timescale is closer to r_0/v. We believe the discrepancy between our results and Roddier is due to the tip/tilt component, which Roddier's calculations do not explicitly remove, but we are planning multilayer simulations to explore this issue. The timescale on which the Taylor "frozen-flow" hypothesis breaks down may also set an upper limit on decorrelation time for large telescopes.

Angel assumes that the speckle halo is completely random from timestep to timestep, and hence the speckles persist only for a time Δt<1ms, an enormous difference. While it seems sensible that speckles introduced by measurement error will be completely random over time Δt, the speckles introduced by fitting error and bandwidth error would in the absence of measurement error clearly be persistent over longer time; the key question is whether the injection of the measurement noise causes the other speckles to be decorrelated.

We addressed this question with simple simulations. A single stationary Kolomogorov phase screen was generated and used for the duration of the simulation – in effect freezing the atmospheric turbulence, so that the only timescale present was that introduced by the AO system. The fitting process was simulated by convolving the measured phase screen with a spatial filter representing the actuator response of the deformable mirror – for these simulations we used a simple gaussian of FWHM=d, though a more complex sinc response similar to existing Xinetics mirrors produced similar results. Wavefront sensor noise was simulated by injecting white noise into the measured wavefront before the convolution, scaled to achieve a given level of additional noise in the final fitted wavefront. The simulations were carried out on a 1024x1024 pixel grid with D=5 m, d=0.05 cm, and a final image scale of 0.25 λ/D per pixel to ensure good sampling in both pupil and image planes. Diffraction effects are removed by apodizing the pupil edges. Figure 2a shows a simulated image with no injected wavefront noise and only fitting error, σ_{fit} =17 nm for the parameters used. We then ran multiple iterations with the same phase screen and different realizations of the white wavefront noise, σ_{wfs} =20nm. Figure 2b shows the first such iteration, with a different and brighter pattern of speckles. Images from these multiple realizations were added together to simulate long exposures; figure 2c shows 10 iterations, and figure 2d shows 100 iterations – and a final image that has come to precisely resemble the speckle pattern due to fitting error, offset by the average halo brightness due to σ_{wfs}. The speckles present never average out in this simulation (where the atmospheric phase screen is stationary); the presence of wavefront measurement noise does not decorrelate the speckles from other noise sources. Note that these are monochromatic images; in broad-band light the speckles would be radially elongated but the basic scalings would not change. Figure 3 plots the residual image standard deviation inside the control radius as a function of the number of WFS noise iterations; the variance initially scales as the square root of the number of iterations (shown by the dotted line) but ultimately reaches a plateau, shown by the dashed line, at a level equal to the image-plane noise in an image with only fitting error. In summary, speckles due to wavefront measurement error do decorrelate rapidly but speckles due to fitting and bandwidth error will persist, decorrelating only on the atmospheric timescale t_{spec}.

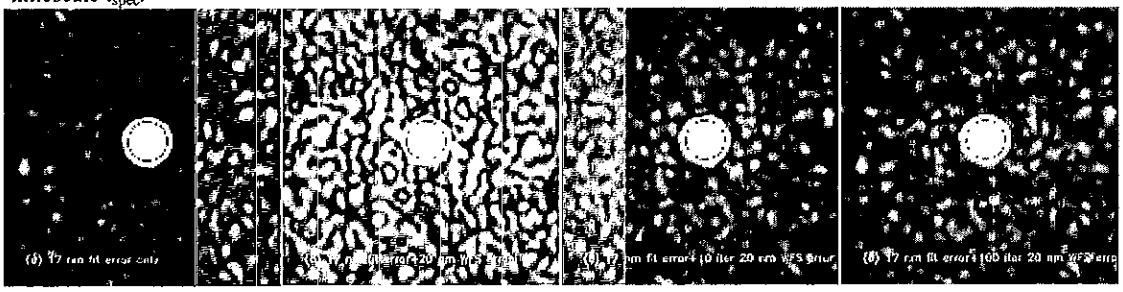

Figure 2a: Simulated PSF with fitting error only. Image is 1.5" on a side.

Figure 2b: Simulated PSF with fitting error + 1 iteration WFS error

Figure 2c: Simulated PSF with fitting error + 10 iterations of WFS error

Figure 2d: Simulated PSF with fitting error + 100 iterations WFS error

On the face of it this appears to contradict Stahl & Sandler[4], whose simulations – much more detailed than ours – showed image-plane noise continuing to decrease over many timesteps Δt. It is possible that the case they simulate involves a sufficiently dim star and sufficiently realistic treatment of wavefront sensor noise that σ_{wfs} simply dominates over other terms; the residual fitting speckles may be decorrelating slowly but they are completely invisible. The somewhat coarse sampling of their simulations may help to decrease the effect of σ_{fit}. It is worth noting that in Stahl and Sandler's initial simulations, when they included additional timelag in their control system, the speckles due to σ_{bw} dominated and persisted over many Δt; only when a simulated predictive controller was used to reduce the effects of σ_{bw} did the noise begin to decorrelate. This shows that even in Stahl and Sandler's detailed simulations speckles due to bandwidth effects are persistent over long timescales. Alternatively, if the hypothesis of Roddier[7] is correct, the primary

difference could be in the use of multiple atmospheric layers in Stahl&Sandler's simulations causing rapid decorrelation of residual speckles. We plan to explore this in our next set of simulations.

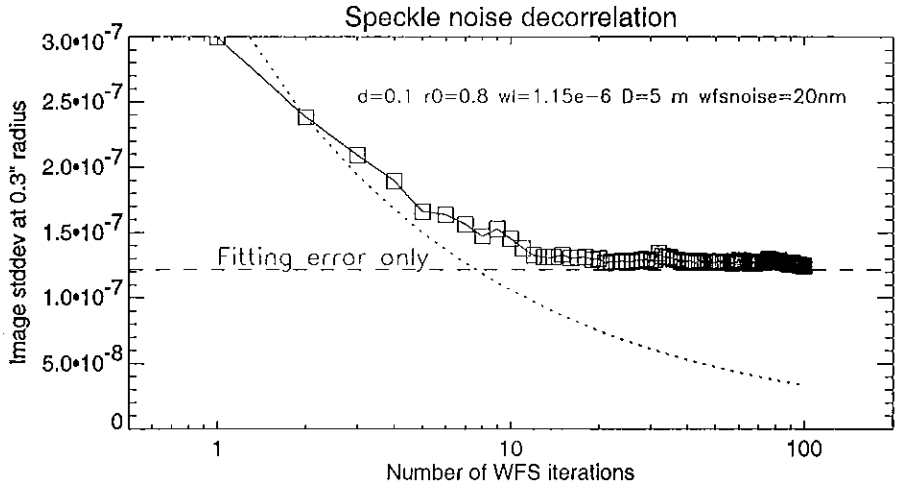

Figure 3: Residual image-plane intensity fluctuations as a function of number of iterations of WFS white noise, for the case described above.

Since the ultimate metric of planet detectability is the image-plane noise in the halo, this leads to a different optimization than that discussed in section 2.2. The image plane noise in a long-exposure image will be given by

$$\text{noise} \propto \text{averaged speckle intesnsity} = \left(\left(\frac{1}{F_s q \Delta t} \right) \left(\frac{\Delta t}{t_{int}} \right)^{1/2} + \left(g \frac{d^{11/3}}{r_0^{5/3}} \right) \left(\frac{t_{spec}}{t_{int}} \right)^{1/2} + \left(w \frac{\Delta t}{r_0} \right)^{5/3} d^2 \left(\frac{t_{spec}}{t_{int}} \right)^{1/2} \right) \quad (5)$$

Since $t_{spec}/\Delta t \approx 100 - 1000$, this has the effect of severely penalizing fitting and bandwidth errors, the second and third terms above, relative to sensing error, and hence driving the optimal system, even in the presence of readout noise, to even small values of d. The optimal d for D=10m is as small as 0.4 cm, an AO system with n=4,000,000 subapertures. Overall signal-to-noise ratios are substantially worse than those predicted by Angel. Practical systems will most likely have d limited by available technology for the foreseeable future. One hopeful result, though, is that the dependence of the final SNR on Δt is quite weak, especially for d larger than the optimum, which reduces the need for extremely fast computation. Another important result is that since the latter two terms dominate the noise for most d values, the dependence on r_0 is quite steep; ExAO performance will be extremely site-dependent. Constructing an ExAO system at a site with better r_0, such as Mauna Kea, will sharply improve performance, and somewhat compensate for the effects of a more realistic decorrelation timescale. The dependence of performance on d is relatively weak once a threshold is reached, with a broad plateau where decreasing d has little effect on performance.

We are using a scaling model based on the above work to predict ExAO performance. Table 1 shows some of the results. One interesting consequence that can be seen is that for a fixed number of actuators n, there exists an optimal telescope size for ExAO, because of the strong dependence on subaperture size d – for a n=30,000 system the optimal D=6.5-8m, though such a system is marginal for planet detection under any circumstances; for n=200,000 the optimal D=15-20m.

The following table lists some calculated signal-to-noise ratios for a planetary companion with a contrast ratio of 10^9 and a separation of 0.5" based on the scaling laws from this paper and from Angel[3]. Other parameters are λ=0.9 μm, bandwidth $\delta\lambda$=0.15 μm, r_0=0.5 m at the observation wavelength (equivalent to above-average Mauna Kea seeing), integration time of 4 hours, wavefront sensor readout noise of 2 electrons per pixel, sensor QE of 0.5, and turbulence-weighted wind of 60 km/h. Segmentation effects (see next section) have been neglected. The first eight cases illustrate

telescope size effects in terms of final SNR for n=31,400 and n=196,000 AO systems; the last show the effects of varying d on the limiting star magnitude for which the target planet can be detected at the 5-sigma level, showing how a broad plateau from d=3 cm to d=0.2 cm, and suggesting that a practical ExAO system could be built around n=100,000.

D (m)	D (m)	n actuators	Δt (ms)	m_{star}	SNR_{planet}
10	0.050	31,400	0.08	2	3.9
8	0.040	31,400	0.11	2	4.4
6.5	0.033	31,400	0.15	2	4.3
5	0.025	31,400	0.22	2	3.4
10	0.020	196,000	0.27	2	18
8	0.016	196,000	0.35	2	12
6.5	0.013	196,000	0.45	2	8.6
5	0.010	196,000	0.62	2	5.2
10	0.048	34,000	0.05	0.9	5
10	0.040	49,000	0.18	2.9	5
10	0.030	87,000	0.35	3.4	5
10	0.020	196,000	0.63	3.7	5
10	0.010	785,000	1.5	3.8	5
10	0.005	3,000,000	3.5	3.9	5
10	0.002	20,000,000	7.8	3.8	5

Table 1: ExAO system performance

4. TECHNOLOGY FOR EXTREME AO SYSTEMS

The rapid advance of adaptive optics technology is one of the main reasons for re-examining the design of planet-detecting AO systems. There are three main technological requirements: a wavefront correction device, a wavefront sensing device, and a reconstruction computer.

The correction requirements are the furthest advanced from the state of the art – current deformable mirrors (DMs) have up to ~1000 controlled actuators, where a ExAO system will require 10^4 to 10^6. Silicon micro-electro-mechanical systems (MEMS) are the most promising technology for this. Assembled with lithographic techniques, MEMS deformable mirrors[8] should in principle scale rapidly to very large actuator counts. Although early MEMS devices have had poor surface quality, this is rapidly improving. Prototype MEMS mirror layers assembled with single-crystal silicon (SOI) wafers have shown surface quality better than 10 nm peak-to-peak[9] [10]. MEMS will most likely lack the large stroke needed to fully correct for atmospheric turbulence, but since the bulk of the power in such turbulence is at low frequencies, a hybrid design with a conventional deformable mirror for low-order/high-power correction and a MEMS for fine correction is practical.

Wavefront sensing with d=1-5 cm is also challenging. Conventional Shack-Hartmann sensors lose sensitivity as d becomes small, as the spot size on each subaperture becomes diffraction-limited and grows with decreasing d. The direct Mach-Zender interferometer proposed by Angel[3] has many advantages, providing a precise, direct phase measurement taking advantage of the coherence of the incoming starlight. The pyramid wavefront sensor[11] is another possibility, as it takes advantage of the full-aperture diffraction limited spot for sensing, though it would likely be more sensitive to calibration issues for non-common-path optics than the M-Z. The AO system will require careful optical design to minimize non-common-path errors, but this level of precision has been demonstrated in applications such as prototype EUV lithography systems.

Computational requirements for a matrix-multiplication reconstruction scale as n^2. More sophisticated reconstruction algorithms such as Fourier-domain reconstruction (computation dominated by the Fourier transform and scaling as $n\log n$) or sparse-matrix multiplication would likely be more efficient for large n. The direct phase measurement of the M-Z interferometer has the considerable advantage of scaling only linearly with n.

5. TELESCOPE SELECTION AND SEGMENTED TELESCOPE EFFECTS

The largest optical/IR telescopes currently operational, the 10-m W.M. Keck telescopes, have primary mirrors composed of 36 contiguous hexagonal segments of diameter d_{seg}=1.8m. While most other 8-m class telescopes have continuous mirrors, it is likely that future 20-100 m telescopes will have Keck-like segmented mirrors. For this reason, and since telescope size has a significant effect on ExAO sensitivity, it is worth studying the effects of mirror segments on ExAO sensitivity. Segmented telescopes have aberrations due to distortions within each individual segment (50-80 nm RMS wavefront error for current Keck mirror segments, based on high-resolution Shack-Hartmann measurements) and due to tip/tilt/piston static errors and vibrations of entire segments (approximately 70 nm RMS for the Keck telescope)[12],. Figure 4 shows a simulated phase map of the Keck telescope, created from S-H measurements of six segments that have been replicated in random orientations to populate the entire mirror. The total RMS phase error is approximately 80 nm, while the peak-to-peak error is 800 nm.

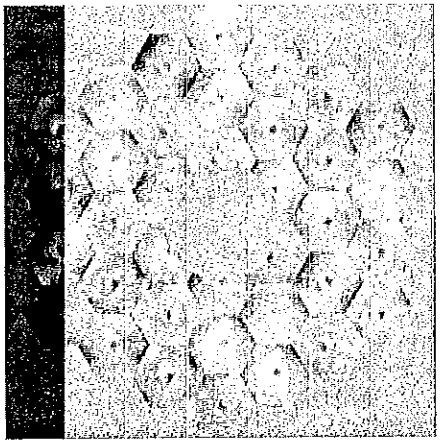

Figure 4: Keck primary mirror phase map (simulated from 6 segments with high-resolution measurements.) Black to white represents ±0.5 micron.

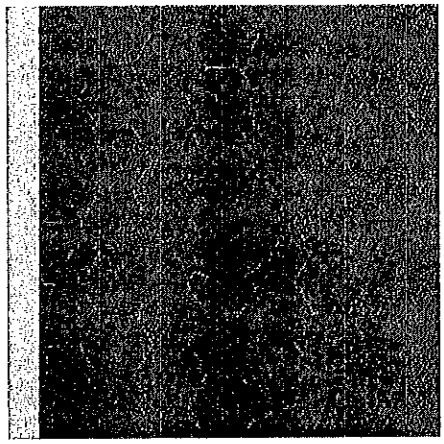

Figure 5: Keck primary mirror phase map after correction by d=5cm ExAO system. Black to white represents ±0.1 micron

The surface and tip/tilt/piston errors of an individual segment do not present a significant problem for ExAO; low spatial frequency errors are easily corrected. Much more problematic are the phase discontinuities across segment boundaries. Tip/tilt/piston errors will introduce sharp discontinuities, but even with perfectly aligned segments, the presence of low-order aberrations across the segment will make it impossible to precisely align each edge of each segment. Almost all ExAO deformable mirrors will be incapable of fitting such a discontinuity, introducing a region of approximate width d over which phase errors are very large. Figure 5 shows the simulated phase map from figure 4 after ExAO correction by a DM with d=5 cm. The RMS phase error has been reduced by a factor of twenty, to 4 nm, but the peak to peak error is only reduced to 240 nm. This produces a grid of bad phase regions tracing the edges of the segments. This grid in turn results in an image with highly regular structure of bright speckle-like features (Figure 6). The features are strongest within a radius given by λ / d_{seg}=0.1 arcseconds, but bright outside this radius, ultimately forming six wide diffraction spikes oriented perpendicular to the segment boundaries. These speckle-like structures have intensity 10^{-8} to 10^{-7} of the peak intensity in monochromatic light, brighter than target extrasolar planets. Although PSF subtraction techniques and observing modes that take advantage of the difference between pupil and sky orientation in an alt/az telescope will help to surpress these effects, it seems unlikely that more than a factor of 10 surpression is possible; ideally, these persistent artifacts should be reduced to below the 10^{-9} level.

This could be achieved in several ways. One approach is a classical Lyot coronagraph, in which a combination of a focal-plane stop and a pupil-plane mask tracing the segment edges blocks diffracted light. (A pupil-only mask would not work, as diffraction off the edges of the pupil would be as bright as the original PSF artifacts.) The inverse relationship between focal-plane stop size and pupil stop size in such a coronagraph[13] would require a focal stop of

radius 0.25 – 1 arcsecond if less than 50% of the pupil is to be blocked; a detailed coronagraph design is outside the scope of this paper. Careful transmission apodization of the pupil mask would improve throughput. Exotic phase-based coronagraphs[14 15] in combination with a narrower Lyot mask could achieve similar results with little or no focal-plane obstruction.

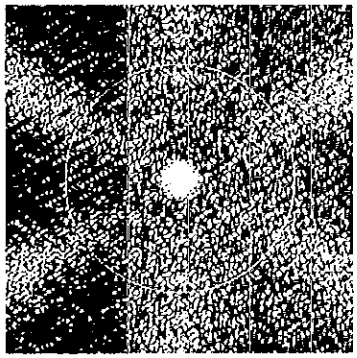

Figure 6a: Simulated Keck AO PSF with real Keck phases (Figure 4) corrected by d=5cm AO system (Figure 5), no atmospheric turbulence. Circle is 1" in diameter and white corresponds to an intensity of 10^{-8} of the peak.

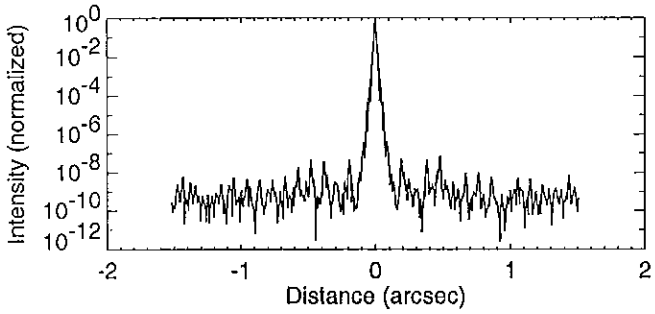

Figure 6b: Intensity profile of a horizontal slice through the center of the image in 6(a), normalized to the peak inesnity.

Alternatively, segmented MEMS could be used to match the segmented telescope – a hexagonal MEMS device to remove segment tip/tilt/piston, or even a mutilayered MEMS in which a continuous-facesheet MEMS is layered on top of a hexagonal segment that is independently controllable. Macroscopic DMs have been proposed in similar configurations.

Although this might argue that a continous-mirror 8-m telescope is a better choice for ExAO than the segmented Keck telescope, careful consideration is needed. ExAO sensitivity has a very steep r_0 dependence since fitting error terms generally dominate, hence an ExAO system should be placed at the best possible site – currently, Mauna Kea. An ExAO system located at a large Naysmith platform should be more stable and easier to calibrate than one subject to gravitational flexure in a Cassegrain location; the Gemini 8-m telescope lacks a Naysmith instrument port. Finally, future large telescopes on the Earth or in space are likely to have segmented mirrors with similar (though hopefully smaller) errrors, and development of an ExAO system on existing segmented telescopes could serve to prototype the coronagraphic techniques that will be needed. The telescope selection question therefore remains open pending more detailed design studies. The CfAO will be carrying out ExAO conceptual designs for several telescope and AO system combinations over the next year.

6. CONCLUSIONS

Direct detection of photons reflected by an extrasolar planet would be a tremendously exciting new development, opening up a new window on other solar systems – including the possibility of seeing systems that resemble our own. In the years since this was first proposed, AO technology has advanced rapidly, and it is now possible to begin to design such systems for practical implementation. Actual performance is likely to be somewhat more pessimistic than that set out in the original Angel paper, primarily due to speckle decorrelation timescales, though careful site selection can mitigate this. The exact value of the speckle decorrelation time is still somewhat unclear and needs to be explored with multi-layer simulations.

Segment-edge phase discontinuities can significantly reduce ExAO performance, but this could be overcome through coronagraphic techniques. In spite of all these effects, ExAO systems with 10^5 actuators still seem capable of planet detection on 8-10m telescopes for target stars brighter than m=4. The NSF Center for Adaptive Optics is working

to produce an ExAO conceptual design over the next year, and one could imagine constructing such a system over the next 3-5 years.

ACKNOWLEDGEMENTS

The authors would like to thank Richard Dekany for organizing a CfAO workshop on ExAO that motivated us to re-examine the scaling laws in Angel (1994), and Mitch Troy for helpful comments on the manuscript. This research was performed under the auspices of the U.S. Department of Energy by Lawrence Livermore National Laboratory under Contract W-7405-ENG-48, and also supported in part by the Center for Adaptive Optics under the STC Program of the National Science Foundation, Agreement No. AST-9876783

REFERENCES

[1] Marcy, G. and Butler, R. P., "Detection of extrasolar giant planets", *Annual Reviews of Astronomy and Astrophysics*, **36**, pp. 57-98, 1998
[2] Macintosh, B., Zuckerman, B., Kaisler, D., Becklin, E., Lowrance, P., Webb, R., Weinberger, A., Schneider, G., Christou, J., "Keck adaptive optics imaging of TWA5 and 6", 2001, to appear in *Young Stars Near Earth*, ASP Conference Series, R. Jaywaharda, ed., 2001
[3] Angel, J. R. P., "Ground based imaging of extrasolar planets using adaptive optics", *Nature*, **386**,pp. 203, 1994
[4] Stahl, S. & Sandler, D., "Optimization and performance of adaptive optics for imaging extrasolar planets", *Astrophysical Journal*, **454**, pp. L153, 1995
[5] Dekany, R., private communication, 2001
[6] Olivier, S., Max, C.E., Brase, J. M., Gavel, D. T., Macintosh, B., Carrano, C., "Direct Imaging of Extra-solar Planets",, *Proceedings International Workshop on Brown Dwarfs and Extra-Solar Planets*, ASP Conference Series **134**, pp. 262, Rebolo, Martin, and Osorio, eds. 1998
[7] Roddier, F., Gilli, J., Lund, G., "On the origin of speckle boiling and its effects in stellar speckle interferometry", *J. Optics (Paris)*, **13**, pp. 263, 1982
[8] Olivier, S., these proceedings, 2001
[9] Carr, E., private communication, 2001
[10] Graff, J., and Schubert, E., "Flat free-standing silicon diaphragms using silicon-on-insulator wafers", *Sensors and Actuators*, **84**, pp. 276, 2000
[11] Ragazzoni, R., Ghedina, A., Baruffolo, A., Marchetti, E., Farinato, J., Niero, T., Crimi, G., Ghigo, M., "Testing the pyramid wavefront sensor on the sky", *Proc. SPIE* **4007**, p. 423
[12] M. Troy, G. A. Chanan, E. Sirko, and E. Leffert, ``Residual misalignments of the Keck telescope primary mirror segments: classification of modes and implications for adaptive optics," L. M. Stepp, ed., Advanced Technology Optical/IR Telescopes VI, vol. 3352, SPIE, pp. 307-317, 1998
[13] Sivaramakrishnan, A., Koresko, C., Makidon, R., Berkefeld, T., Kuchner, M., "Ground-based coronagraphy with high-order adaptive optics", *Astrophysical Journal*, **552**, pp. 397, 2001
[14] Baudoz, P., Rabbia, Y., Gay, J., "Achromatic interfero coronagraphy I. Theoretical capabilities for ground-based observations", *Astronomy and Astrophysics Supplement*, **141**, pp. 319, 1999
[15] Rouan, D., Riaud, P., Boccaletti, A., Clenet, Y, Labeyrie, A., "The Four-Quadrant Phase-Mask Coronagraph. I. Principle", *Publications of the Astronomical Society of the Pacific*, **112**, pp. 1479-1486, 2000